

Harmonic Suppression by Using T-shaped Spur-Line in a Compact Hairpin-Line Bandpass Filter

Tarun Kumar DAS¹, Sayan CHATTERJEE²

¹ Dept. of Electronics and Communication Engg., Future Institute of Engg. and Mgmt., Sonarpur, Kolkata, India

² Dept. of Electronics and Telecommunication Engg., Jadavpur University, Jadavpur, Kolkata, India

tarunj1979@gmail.com, sayan1234@gmail.com

Submitted October 17, 2020 / Accepted March 2, 2021

Abstract. *This article exhibits the design of a fourth-order compact hairpin-line bandpass filter centered at 2.5 GHz and with a 3 dB fractional bandwidth of 5% along with a sharp roll-off factor and wide stopband characteristics required for Wireless Local Area Network (WLAN). Miniaturization of the conventional hairpin-line filter has been achieved by folding the open end arms twice towards the inward direction and accordingly, a size reduction of 42% has been obtained. Subsequently, T-shaped spur-lines with optimum dimensions have been incorporated at both the inner and outer edges of the coupled arms of the folded hairpin-line cell. Accordingly, two fourth-order folded filters with outer T-shaped and double T-shaped spur-lines have been designed and verified experimentally. An extended stopband with a rejection level of 39 dB up to $3.2f_0$ along with a size reduction of 46% has been achieved.*

Keywords

Folding, hairpin-line filters, spur-line, harmonic suppression, wide stopband

1. Introduction

In the modern-day communication world, the Internet of Things (IoT) enables users to transfer data efficiently and securely over the communication channel. In Wireless Local Area Network (WLAN) receivers for IoT connectivity, narrowband and compact bandpass filters play an important role to allocate the desired signals within the limited frequency range. However, the design of such a filter becomes a challenging issue for the researchers for the last decades due to the design and fabrication difficulties along with the presence of spurious harmonics. Accordingly, the conventional hairpin-line filter topology has been employed extensively [1]. However, the conventional filters still acquire a large floor plan, not suitable for modern wireless communication systems. Later, the conventional hairpin-line filter has been modified to a cross-coupled filter to achieve more compactness and high skirt characteristics by employing hybrid coupling [2]. Later, two

open-loop resonators have been loaded with stubs in [3] to design a bandpass filter with improved out-of-band characteristics of 50 dB rejection level. In this context, several absorptive lossy filters for satellite receivers based on hairpin-lines have been investigated in [4]. However, the sizes of the filters are quite large, restricting their application in modern-day's satellite receivers. Moreover, in [2–4] the harmonic suppression characteristics of the filters have not been addressed. In this context, different types of perturbations have been introduced in hairpin-line filters to achieve a wide stopband. In general, two approaches have been investigated for harmonic suppression of filters by (1) shifting the harmonics to higher frequency regions by cascading a low-pass filter [1] and (2) introducing transmission zeros at the locations of the harmonics and reducing the attenuation levels accordingly by different types of perturbations to achieve modal phase velocity compensation. However, the introduction of a low-pass filter has increased the overall filter size greatly. In this context, the harmonic suppressed hairpin-line filters have been designed with Koch fractals [5] (stopband rejection level of 29 dB up to $2f_0$ where f_0 is the center frequency), split-mode excitations [6] (20 dB up to $8.33f_0$), Defected Microstrip Structure (DMS) [7] (33 dB up to $3.4f_0$), and Minkowski fractals [8] (30 dB up to $2f_0$). However, the design and fabrication difficulties are increasing as the iteration order of these types of perturbations increases. Although the harmonic suppression characteristics of the above filters [5–8] are satisfactory, the sizes of the filters are quite large due to their conventional hairpin-line filter structures, restricting their applications. Afterward, in [9] $\lambda/4$ and $\lambda/2$ stepped-impedance resonators have been employed to design a 96% size reduced compact filter with a wide stopband of rejection level of 30 dB up to $3f_0$. Recently, in [10] a short-stub-loaded dual-mode resonator (SSL-DMR) and two stepped-impedance spur-line resonators (SISLRs) have been employed to achieve size miniaturization and a wide stopband of rejection level of 20 dB up to $4f_0$. Recently, a folded hairpin-line filter centered at $2.5f_0$ has been proposed in [11] where periodic rectangular grooves with optimum dimensions have been incorporated into the coupled-edges. Accordingly, more than 33 dB of stopband rejection level up to $2.2f_0$ along with a size reduction of

25% has been achieved. However, the design of narrow-band compact filters with improved selectivity and wide stopband with a rejection level of more than 35 dB is still a challenge.

In the present article, the study of [11] has been extended to achieve more compactness and harmonic suppression performance for the folded hairpin-line bandpass filter (FHLBF) by reducing the cross-coupling area between the folded arms. Subsequently, the coupled-arms of the adjacent folded hairpin-line (FHL) cells have been perturbed by the T-shaped spur-line to achieve modal phase velocity compensation and suppress the attenuation levels of the harmonics. The dimensions of the spur-line have been adjusted from the parametric study and the length of the resonators has been tuned to maintain the passband characteristics. To validate the design scheme, two fourth-order folded filters centered at 2.50 GHz with a fractional bandwidth of 5% suited for WLAN (IEEE802.11b) applications, have been designed with T-shaped spur-lines. The filter has been designed on FR4 epoxy substrate having dielectric constant, $\epsilon_r = 4.4$, loss tangent, $\tan\delta = 0.02$, and thickness, $h = 1.6$ mm. As a result, an upper stopband rejection level of more than 39 dB has been obtained up to $3.2f_0$ along with a size reduction of 46%.

2. Folding of the Hairpin Resonator

2.1 Resonance Property of Unit Folded Cell

The conventional half-wavelength hairpin-line has been folded at its open-end arms symmetrically twice to the inward direction as shown in Fig. 1. The unit FHL cell has been characterized by the different design dimensions of l_1 , l_2 , S , w , and d . For simplicity of the design, uniform spacing (S) has been considered for the entire folded structure. The optimum value of the cross-coupling gap (d) between the folded arms of a hairpin-line has been chosen as 0.3 mm from the design curve shown in Fig. 2. It has been observed from Fig. 2 that the resonant frequency increases nonlinearly with the incremental value of d . This is owing to the reduction in the coupling area between the parallel-coupled folded arms. The FHL cells have been cascaded in hybrid mode to design the higher order folded filter as discussed in the next section.

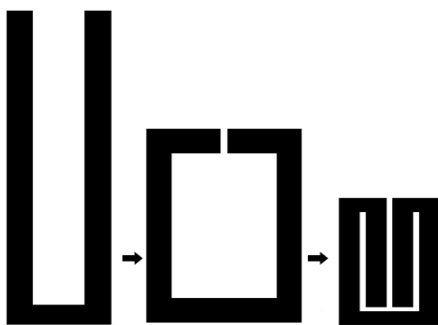


Fig. 1. Folding mechanism of the hairpin resonator.

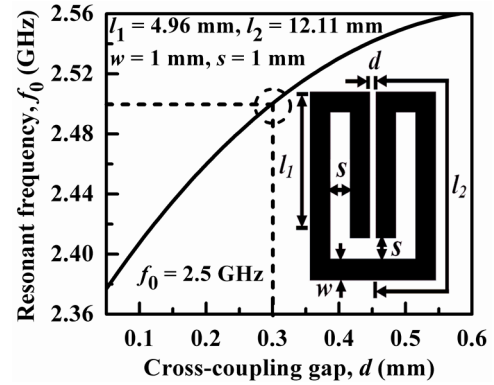


Fig. 2. Variation of resonant frequency (f_0) vs. cross coupling gap (d) for a unit FHL cell.

2.2 Design of Fourth-order Folded Filter

The proposed Chebyshev-type bandpass filter has the specifications of center frequency, $f_0 = 2.50$ GHz, fractional bandwidth, $FBW = 5\%$, 3 dB passband frequency range of 2.438 GHz–2.563 GHz, passband ripple, $L_{Ar} = 0.01$ dB. The order of the filter has been calculated as four by following the conventional filter theory [1]. The external quality factors of the first and fourth resonators and the coupling coefficients between the adjacent resonators are obtained as $Q_{e1} = Q_{e4} = 14.258$, $M_{1,2} = M_{3,4} = 0.0541$, $M_{2,3} = 0.0397$. The width of the tapped-line feed-ports has been calculated as 3.06 mm corresponding to the characteristic impedance of 50 Ω . The initial values of coupling gaps between the adjacent cells have been extracted from the design curve of Fig. 3 (marked by A and B) as $s_{1,2} = s_{3,4} = 1.03$ mm for $M_{1,2} = M_{3,4} = 0.0541$, and $s_{2,3} = 1.33$ mm for $M_{2,3} = 0.0397$. Figure 4 shows the layout of the fourth-order folded filter with optimized dimensions in mm. The size of the filter is 328.35 mm² i.e., $0.51\lambda_0 \times 0.14\lambda_0$ and accordingly, a size reduction of 42% has been achieved over the conventional filter. Figure 5 compares the simulated S -parameters between the conventional and folded hairpin-line filters.

It has been observed that two sharp transmission zeros (TZ_{f1} and TZ_{f2}) have been obtained for the folded filter at 3.7 GHz and 5.75 GHz with an attenuation level of 67 dB and 56 dB. Besides, the second harmonic frequency

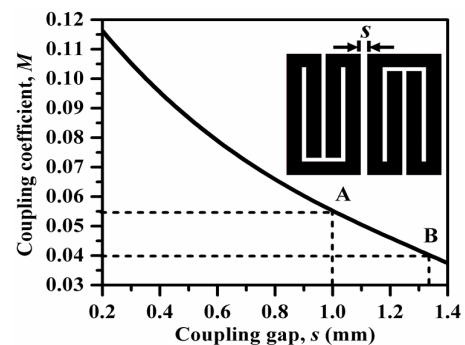


Fig. 3. Design curve obtained by full-wave EM simulations for the coupling coefficient, M for the folded hairpin-line bandpass filter.

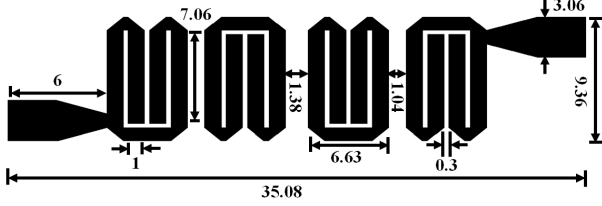


Fig. 4. Layout of the fourth-order folded hairpin-line bandpass filter.

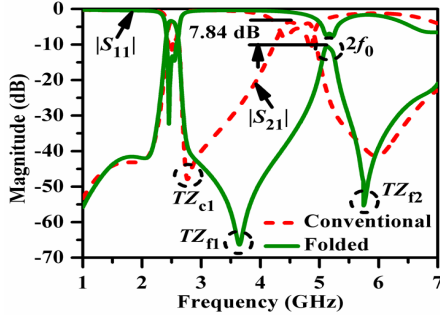


Fig. 5. Comparison of S -parameters plots between the conventional and the folded hairpin-line filters.

($2f_0$) has been shifted to 5.25 GHz from 4.7 GHz with degradation in the attenuation level of 6.8 dB. This has been occurred due to the reduction in the effective coupling area between the adjacent coupled-arms as well as the additional strong cross-coupling inside the cell. Accordingly, the inclusion of spur-lines at the coupled edges of the adjacent resonators and its effects on harmonic suppression performance has been studied in the following section.

3. Harmonic Suppression by Spur-Line

In general, the spur-line is a simple defected structure, which is realized by etching an L-shape slot on the top microstrip line [12]. Moreover, a pair of coupled lines is included with both lines connected at the ends. The spur-line open-end gap capacitance is denoted by C_{sp} . Without any stubs and etched processing on the backside ground plane, it can provide excellent wideband rejection characteristics and can be applied in compact filter designs. Compared to the conventional open-circuited shunt-stub and coupled-line filters, spur-line-based filters are of very compact structures. Moreover, they exhibit less radiation, more susceptibility to nearby elements, virtually non-dispersive behavior, i.e. the resonance characteristics are solely determined by the odd-mode of propagation [13]. The equivalent chain matrix of the conventional L-shaped spur-line is expressed by assuming $\theta_{0o} = \theta_{0e} = \theta$ as (1). In (1) Z_{0o} and Z_{0e} are the odd- and even-mode characteristic impedances, θ_{0o} and θ_{0e} are the odd- and even-mode electrical lengths respectively of the coupled line section.

$$\begin{bmatrix} A & B \\ C & D \end{bmatrix} = \begin{bmatrix} \cos \theta & j \left(\frac{Z_{0o} + Z_{0e}}{2} \right) \sin \theta \\ j \frac{2}{Z_{0e}} \sin \theta & \cos \theta - \frac{Z_{0o}}{Z_{0e}} \sin \theta \tan \theta \end{bmatrix}. \quad (1)$$

Here, the terminal voltage conditions are $V_1 = V_2 = V_A$, $V_3 = 0$ and $V_4 = V_B$. The T-shaped spur-line structure has been obtained by placing two L-shaped spur-lines opposite to each other about the symmetry line in the middle as shown in Fig. 6(a), (b). The equivalent chain matrix is obtained accordingly as

$$\begin{bmatrix} A_T & B_T \\ C_T & D_T \end{bmatrix} = \begin{bmatrix} A_L & B_L \\ C_L & D_L \end{bmatrix} \cdot \begin{bmatrix} D_R & B_R \\ C_R & A_R \end{bmatrix} \quad (2)$$

$$\begin{bmatrix} A_T & B_T \\ C_T & D_T \end{bmatrix} = \begin{bmatrix} 1 - 2k \sin^2 \theta & jkZ_{0e} \sin \theta \cos \theta \\ j \frac{4 \tan \theta}{Z_{0e}} (1 - k \sin^2 \theta) & 1 - 2k \sin^2 \theta \end{bmatrix} \quad (3)$$

$$\text{where} \quad k = \frac{Z_{0e} + Z_{0o}}{Z_{0e}}. \quad (4)$$

The suffix T stands for total; L stands for the left side and R stand for the right side of the symmetry line of the spur. The equivalent $|S_{21}|$ has been derived by the parameters conversion [1] and expressed as

$$|S_{21}|^2 = \frac{1}{4Z_0^2} (p^2 + q^2 \sin^2 \theta) \quad (5)$$

where

$$p = 2Z_0(1 - 2k \sin^2 \theta), \quad (6a)$$

$$q = kZ_{0e} \cos \theta + \frac{4Z_0^2}{Z_{0e}} \cos \theta (1 - k \sin^2 \theta). \quad (6b)$$

Figure 7(a) illustrates the $|S_{21}|$ (dB) plot for the outer T-shaped spur-line structure according to (5) for different values of the spur-line gap, g . The transmission zeros have been obtained under the condition of $\theta = (2i - 1)\pi/2$, for $i = 1, 2, 3, \dots, (2n + 1)$, where n is a positive integer. It has been observed that the small value of g has significantly improved the skirt selectivity of the passband. By following the same method, the equivalent chain matrix of a double T-shaped spur-line as shown in Fig. 6(c), (d) has been determined as (7). The equivalent $|S_{21}|$ has been derived by the parameters conversion and expressed as (8). Figure 7(b) shows the $|S_{21}|$ (dB) plot for a double T-shaped spur-line structure according to (7).

$$\begin{bmatrix} A_{Td} & B_{Td} \\ C_{Td} & D_{Td} \end{bmatrix} = \begin{bmatrix} \frac{1}{1 - 2k \sin^2 \theta} & -j \frac{Z_{0e} k \sin \theta \cos \theta}{2(1 - 2k \sin^2 \theta)} \\ j \frac{8 \tan \theta (1 - k \sin^2 \theta)}{Z_{0e} (1 - 2k \sin^2 \theta)} & \frac{1}{1 - 2k \sin^2 \theta} \end{bmatrix}, \quad (7)$$

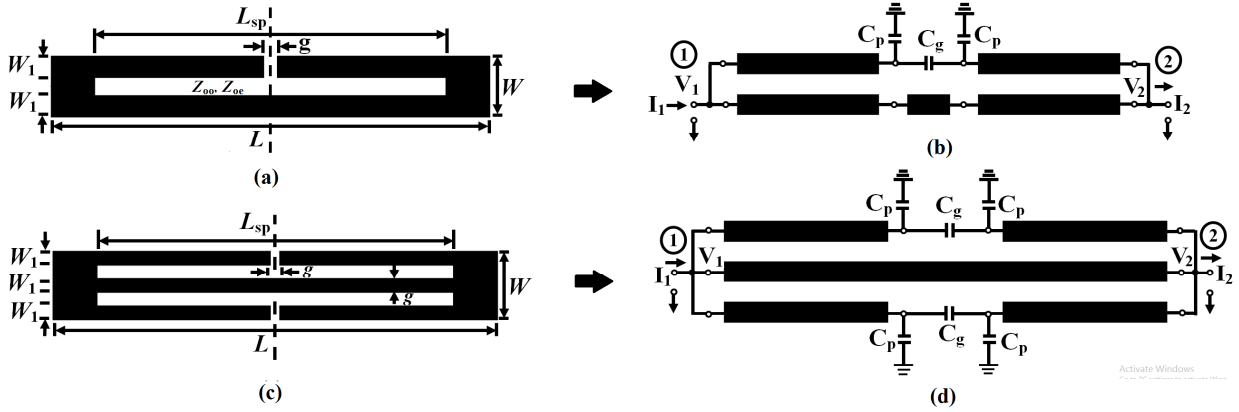


Fig. 6. (a) Layout diagram of outer T-shaped spur-line (OTSP), and (b) transmission line structure. (c) Layout diagram of double T-shaped spur-line (DTSP), and (d) transmission line structure.

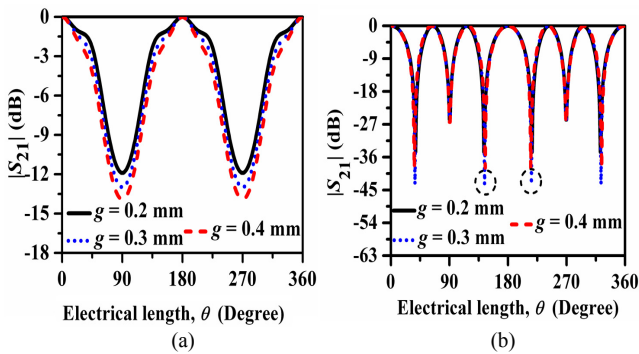


Fig. 7. Variation of $|S_{21}|$ (dB) vs. electrical length, θ (Degree) of the T-shaped spur-line for different values of spur-line gap, g (mm) for (a) OTSP, (b) DTSP based.

where
$$|S_{21}|^2 = \frac{1}{4Z_0^2} (m^2 + n^2 \sin^2 \theta), \quad (8)$$

$$m = \frac{2Z_0}{1 - 2k \sin^2 \theta}, \quad (9)$$

$$n = \frac{16Z_0^2(1 - k \sin^2 \theta) - Z_{0e}^2 k \cos^2 \theta}{2Z_{0e}(1 - 2k \sin^2 \theta) \cos \theta}. \quad (10)$$

The transmission zeros have been obtained under the condition of $\theta = (2i - 1)\pi/4$, for $i = 1, 2, 3, \dots (2n + 1)$, where n is a positive integer. Moreover, it has been observed that the skirt selectivity of the passband of the resonance plots has been improved and bandwidth has been reduced for a DTSP compared to the OTSP structure. Thus, the values of g and θ are to be chosen adequately for desirable bandstop performance to place a transmission zero at the harmonic frequencies.

The effects of spur-line gap capacitance have not been considered in the above analysis as no current will flow across the gap at resonance and the voltage developed across it becomes zero (Fig. 6(a)). In general, a capacitive effect is provided by the spur-line slot and an inductive effect is exhibited by the narrow line. Accordingly, an improvement over the effective inductance and capacitance of the microstrip line has been obtained, resulting in

an increment of the effective permittivity of the dielectric substrate. It can be concluded from this section that the T-shaped spur-line structure exhibits excellent bandstop resonance characteristics by introducing transmission zeros for the appropriate length of the spur-line (θ) along with the optimum value of g . This feature of T-shaped spur-line has been studied further in the following section for the folded hairpin-line cells which are the building blocks of narrowband fourth-order folded filter. The equivalent circuit of the OTSP is shown in Fig. 8(a) where the resonant characteristics are modeled by a parallel RLC resonant circuit. In Fig. 8(a), R has been included for the radiation effect and conductor loss and L resonator have been considered corresponding to the spur-line. Based on the transmission line theory and the spectral domain approach, the circuit parameters can be extracted using the following equations (11)–(13) [13]:

$$R = 2Z_0(1/|S_{21}| - 1)|_{f=f_0}, \quad (11)$$

$$C = \frac{\sqrt{0.5(R + 2Z_0)^2 - 4Z_0^2}}{2.83\pi Z_0 R \Delta f}, \quad (12)$$

$$L = \frac{1}{4(\pi f_0)^2 C}. \quad (13)$$

Here, Z_0 is the 50Ω characteristic impedance of the transmission-line and Δf is the 3 dB bandwidth of simulated $|S_{21}|$.

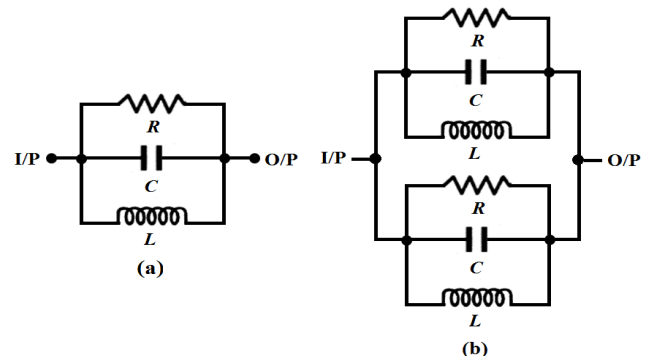


Fig. 8. Equivalent lumped elements circuit diagrams of (a) OTSP and (b) DTSP based spur-line.

The comparison between EM simulated and circuit simulated plots of $|S_{21}|$ (dB) for a half-wavelength OTSP based line with dimensions: $L = 37.64$ mm, $L_{sp} = 37.04$ mm, $W = 1.0$ mm, $W_1 = 0.35$ mm, $g = 0.3$ mm (Fig. 6(a)) and DTSP based line with dimensions: $L = 37.64$ mm, $L_{sp} = 37.04$ mm, $W = 1.0$ mm, $W_1 = 0.35$ mm, $g = 0.3$ mm (Fig. 6(c)) tuned at the resonant frequency, $f_0 = 2.5$ GHz has been illustrated in Fig. 9(a), (b) respectively. The circuit parameters have been calculated by (11)–(13) as $L = 0.410$ nH, $C = 1.929$ pF, $R = 3.125$ k Ω for OTSP based line with $|S_{21}| = 33$ dB at f_0 and $\Delta f = 0.85$ GHz, and $L = 0.301$ nH, $C = 2.626$ pF, $R = 4.167$ k Ω for DTSP based line with $|S_{21}| = 27$ dB at f_0 and $\Delta f = 0.62$ GHz. It has been observed from Fig. 9(a), (b) that the value of Δf for 3 dB insertion loss in circuit simulation has been decreased by 55.8% (from 1.13 GHz to 0.5 GHz) for DTSP based line compared to OTSP based line. This is owing to the increment of the capacitance (C) and decrement of the inductance for the DTSP based line over OTSP based line. However, the

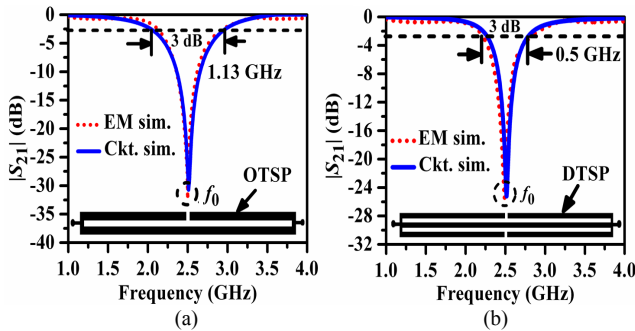


Fig. 9. Comparison of EM simulated vs. circuit simulated $|S_{21}|$ (dB) plots of (a) OTSP and (b) DTSP based spur-line.

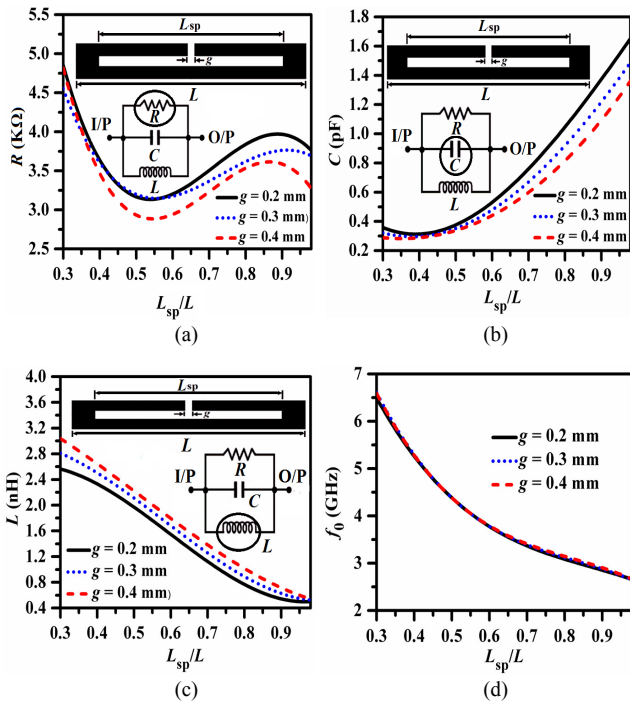


Fig. 10. Variation of (a) R (k Ω), (b) C (pF), (c) L (nH) and (d) f_0 (GHz) for a T-shaped spur-line with incremental length ratio L_{sp}/L .

attenuation level at f_0 has been increased from 33 dB to 27 dB (18.2 %) for DTSP based line over OTSP based line. This has been occurred due to the reduction of effective conducting surface area and hence, the surface current density distribution along the line has been diminished.

Figures 10(a)–(d) show the variation of R (k Ω), C (pF), L (nH) and f_0 (GHz) for a T-shaped spur-line with incremental length ratio, L_{sp}/L . It has been observed that resistance varies asymmetrically due to the variation of the effective surface area of the conductor. The value of C increases exponentially due to the additional cross-couplings in the slot.

The value of L decreases exponentially due to the reduction of the width of the line and f_0 decreases exponentially due to the increment of the effective electrical path of the spur-line. From the above study, it can be concluded that the OTSP based line has exhibited more improvement in the attenuation level at the resonant frequency over the DTSP based line. However, the selectivity of the passband has been improved significantly for the DTSP based line. Accordingly, these unique features of T-shaped spur-line have been utilized for a folded hairpin-line cell to design fourth-order filter as discussed in the next section.

4. Unit FHL Cell with Spur-Line

The structures of a folded hairpin line cell with three different types of T-shaped spur-lines introduced in the coupling arm (right-side) are shown in Fig. 11(a)–(c). The spur-lines have been named as outer T-shaped (OTSP), inner T-shaped (ITSP), and double T-shaped (DTSP) according to their locations. The resonant characteristics of the unit FHL cell with different T-shaped spur-lines have been studied in Fig. 12. It has been observed that the attenuation levels of the second harmonic frequency, $2f_0$ have been degraded for all the cases with a minimum for DTSP based FHL cell. However, the spur-line has a minimum effect on the third harmonic frequency, $3f_0$. Moreover, the fundamental frequency, f_0 has been shifted to a lower frequency region due to the increase in the effective electrical length of the line due to the defected microstrip slot.

The equivalent lumped elements circuit of a unit FHL cell with OTSP based and DTSP based spur-line has been depicted in Fig. 13(a), (b). The right arm of the FHL cell has

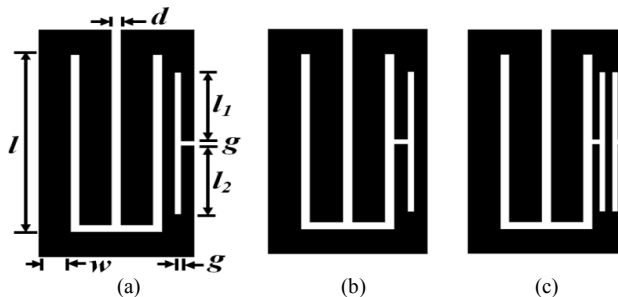


Fig. 11. Layout of unit folded hairpin-line cell with spur-lines: (a) OTSP, (b) ITSP, and (c) DTSP.

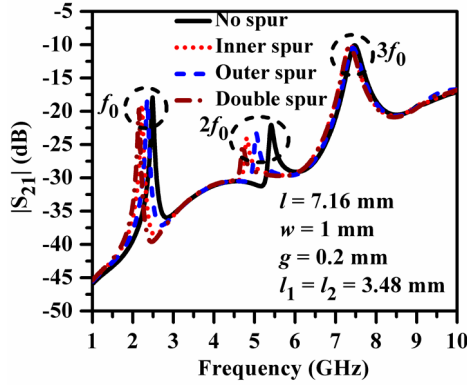


Fig. 12. Comparison of EM simulated vs. circuit simulated $|S_{21}|$ (dB) plots of DTSP based spur-line.

been modified by the equivalent RLC parallel resonant circuit of the outer T-shaped spur-line as shown in Fig. 13(a). It has been noted from Fig. 13(b) that two OTSP based spur-line OTSP-L and OTSP-R have been connected in parallel to obtain a DTSP-based spur-line circuit. Table 1 lists the values of the lumped elements. The value of the resistor has been calculated as $R_{sp} = 3.448$ k Ω . The comparisons between EM simulated and circuit simulated plots of $|S_{21}|$ (dB) for unit FHL cell with OTSP and DTSP based spur-line in Fig. 14(a), (b) respectively. It has been observed that the stopband attenuation level has been degraded more for DTSP based spur-line than OTSP based line. However, the FHL cell with DTSP based spur-line has been exhibited narrow 3 dB bandwidth along with steeper skirt selectivity of the bandstop response.

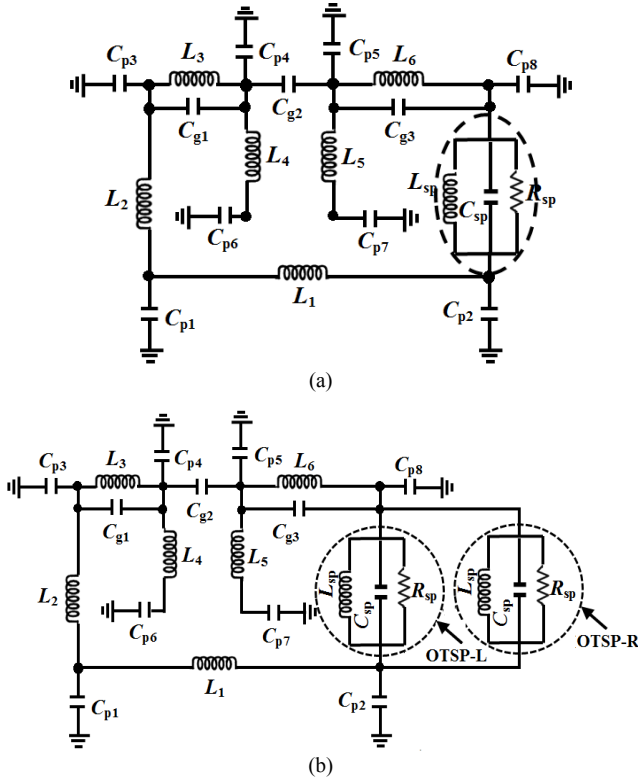


Fig. 13. Equivalent lumped elements circuit of a unit FHL cell with T-shaped spur-line. (a) OTSP based, (b) DTSP based.

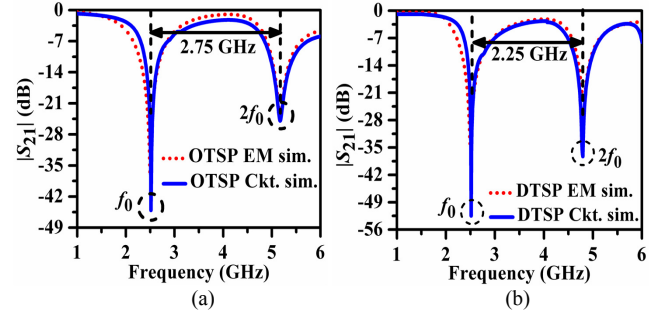


Fig. 14. Comparison of EM simulated vs. circuit simulated $|S_{21}|$ (dB) plots of a unit FHL cell with OTSP based spur-line.

Inductors (nH)		Capacitors (pF)	
L_1	2.426	$C_{p1} = C_{p2}$	0.167
L_2	3.011	$C_{p3} = C_{p8}$	0.287
$L_3 = L_6$	1.169	$C_{p4} = C_{p5}$	0.083
$L_4 = L_5$	3.685	$C_{p6} = C_{p7}$	0.275
L_{sp}	2.305	$C_{g1} = C_{g2} = C_{g3}$	0.015
		C_{sp}	1.738

Tab. 1. Values of the lumped elements.

Moreover, the attenuation level at $2f_0$ has been increased due to the additional inductive and capacitive effects of the DTSP based FHL cell. From this study of FHL cell with T-shaped spur-line, it has been concluded that both DTSP and OTSP spur-line can suppress the higher-order harmonics of the hairpin-line due to its bandstop behavior.

5. Fourth-Order Folded Filter with Spur-Line

The optimum values of length ratio $\alpha = L_{sp}/L$ for maximum second harmonic suppression have been chosen as 0.6 for outer and 0.7 for double T-shaped spur-lines from the parametric study. Accordingly, initial values of the coupling gap between the adjacent FHL cells have been obtained from the design graphs of the coupling coefficient (M) as shown in Fig. 15, marked by A, B for $M = 0.0541$ and C, D for $M = 0.0397$. The layouts of the fourth-order folded filters with OTSP and DTSP are shown in Fig. 16(a), (b) respectively. The sizes of the designed filters are $0.49\lambda_0 \times 0.12\lambda_0$ and $0.49\lambda_0 \times 0.11\lambda_0$ respectively, where λ_0 is the guided wavelength at f_0 . The equivalent lumped elements circuits of the filters have been modeled by cascading the circuits of Fig. 13(a) for OTSP based and Fig. 13(b) for DTSP based. Subsequently, the $|S_{21}|$ (dB) plots have been compared between the EM-simulation and the circuit-simulation in IE3D solver with excellent agreement as highlighted in Fig. 17(a), (b) respectively.

6. Experimental Results

Figures 18(a), (b) show the photographs of the fabricated prototypes of the proposed filters. The experiment

has been carried out in the Agilent N9928A vector network analyzer and the measured vs. simulation $|S_{21}|$ (dB) plots have been highlighted in Fig. 19(a), (b). An extended stopband of rejection levels of 37 dB from 2.87 GHz to 7.5 GHz and 39 dB from 3.0 GHz to 7.8 GHz have been obtained for the OTSP and DTSP based filter. The comparison between measured and simulated $|S_{11}|$ (dB) plots has been illustrated in Fig. 20(a),(b).

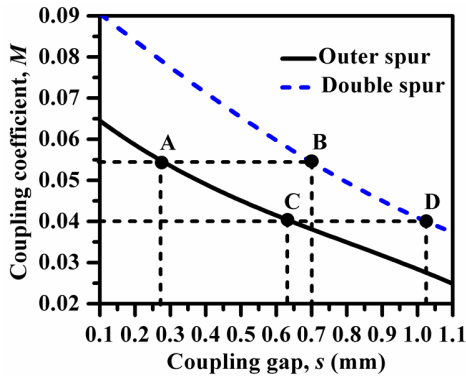


Fig. 15. Design curves for coupling coefficient vs. coupling gap for a pair of FHL cells with spur-line.

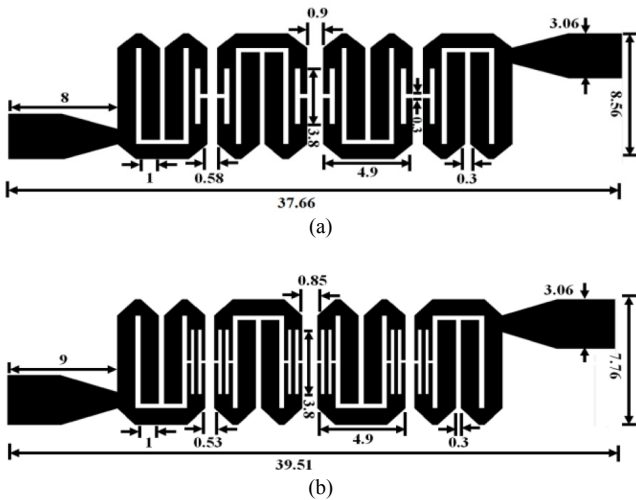


Fig. 16. Layouts of fourth-order folded hairpin-line filters with spur-lines: (a) OTSP based and (b) DTSP based. All dimensions are in mm.

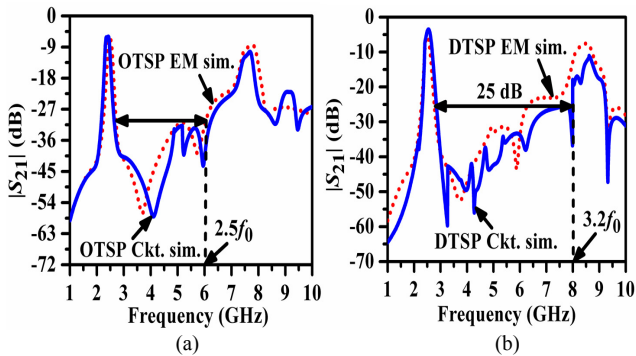


Fig. 17. Comparison of $|S_{21}|$ (dB) plots between EM simulation and circuit simulation for a fourth-order folded filters with (a) OTSP and (b) DTSP based spur line.

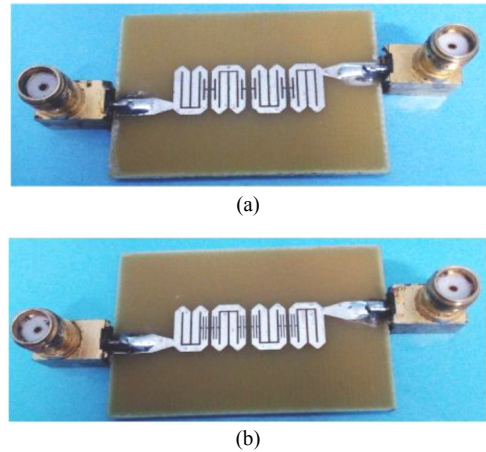


Fig. 18. Fabricated prototypes of filters: (a) OTSP based; (b) DTSP based.

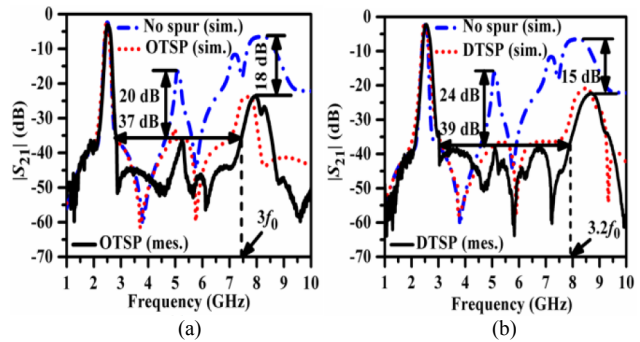


Fig. 19. Comparison between simulated vs. measurements results of $|S_{21}|$ (dB) for folded filters with (a) DTSP based and (b) OTSP based spur-lines.

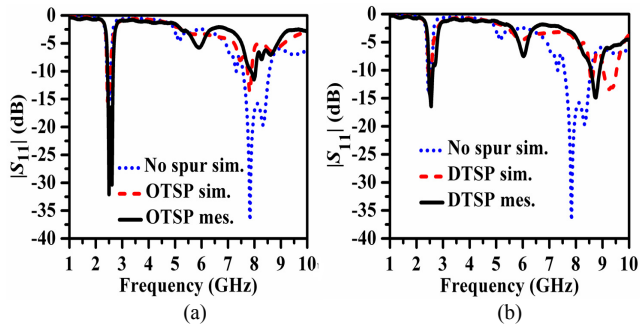


Fig. 20. Comparison between simulated vs. measurements results of $|S_{11}|$ (dB) for folded filters with (a) DTSP based, (b) OTSP based spur-lines.

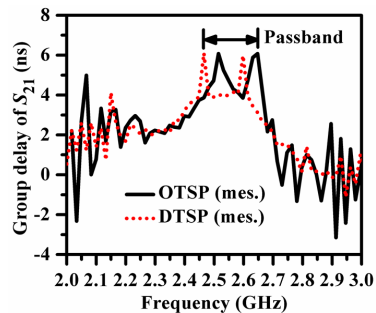


Fig. 21. Comparison between measured group delay (ns) of $|S_{21}|$ for folded filters with spur-line.

Design	f_c (GHz)	SRL (dB)	IL (dB)	SBW (GHz)	Size $\lambda_o \times \lambda_o$
OTSP	2.50	37	2.8	$3.0f_0$	0.49×0.12
DTSP		39	2.9	$3.2f_0$	0.49×0.11
[7]	2.10	33	1.4	$3.4f_0$	0.16×0.75
[8]	1.0	30	1.3	$2.8f_0$	0.34×0.19
[9]	3.50	30	1.7	$3.0f_0$	0.21×0.18
[10]	10.81	20	0.6	$4.0f_0$	0.16×0.75
[11]	2.50	33	2.7	$2.2f_0$	0.45×0.12

Tab. 2. Comparison of similar studies.

The measured insertion loss for the filters is pretty large (> 2.5 dB) due to the lossy FR4 substrate material and tolerances incurred near the SMA connectors and spectrum analyzer during measurement. Figure 21 shows the measured group delay plots of $|S_{21}|$ in ns exhibiting symmetry at the narrow passband edges as an improvement over conventional folded filters without spur-line. Table 2 highlights the comparative study with fractional bandwidth (FBW, %), stopband rejection level (SRL, dB), insertion loss (IL, dB), stopband rejection bandwidth (SBW, GHz) and Size in terms of $\lambda_o \times \lambda_o$. It has been noted that there has been an improvement in the stopband rejection level better than [7–11]. Moreover, the sizes of the proposed filters are more compact than [7], [8], and [10].

7. Conclusion

The design of a folded hairpin-line filter with a T-shaped spur-line has been proposed in the present article. The coupled-arms of the adjacent folded cells have been perturbed by outer and double T-shaped spur-lines to achieve modal phase velocity compensation. As a result, an extended stopband below the rejection level of 39 dB up to $3.2f_0$ has been obtained experimentally for DTSP based filter along with a size reduction of 46%. The proposed filters are applicable to WLAN systems.

References

- [1] HONG, J. S., LANCASTER, M. J. *Microstrip Filters for RF/Microwave Applications*. New York (NY, USA): John Wiley & Sons, 2001, p. 84–86. ISBN 0-471-22161-9
- [2] VAGNER, P., KASAL, M. A novel bandpass filter using a combination of open-loop defected ground structure and half-wavelength microstrip resonators. *Radioengineering*, 2010, vol. 19, no. 3, p. 392–396. ISSN: 1210-2512
- [3] MAHARJAN, R. K., KIM, N. Y. Miniature stub-loaded square open-loop bandpass filter with asymmetrical feeders. *Microwave and Optical Technology Letters*, 2013, vol. 55, no. 2, p. 329–332. DOI: 10.1002/mop.27318

- [4] BASTI, A., PERIGAUD, A., BILA, S., et al. Design of microstrip lossy filters for receivers in satellite transponders. *IEEE Transactions on Microwave Theory and Techniques*, 2014, vol. 62, no. 9, p. 2014–2024. DOI: 10.1109/TMTT.2014.2337285
- [5] BARAL, R. N., SINGHAL, P. K. Design of microstrip band pass fractal filter for suppression of spurious band. *Radioengineering*, 2008, vol. 17, no. 4, p. 34–38. ISSN: 1210-2512
- [6] LIN, W. J., LI, J. Y., LIN, D. B., et al. Multi-suppression of microstrip bandpass filter using split-mode excitations. *Journal of Electromagnetic Waves and Applications*, 2010, vol. 24, no. 11–12, p. 1501–1510. DOI: 10.1163/156939310792149777
- [7] NASER-MOGHADASI, N. M., ALAMOLHODA, M., RAHMATI, B. Spurious response suppression in hairpin filter using DMS integrated in filter structure. *Progress in Electromagnetics Research C*, 2011, vol. 18, p. 221–229. DOI: 10.2528/PIERC10110914
- [8] LOTFI-NEYESTANAK, A. A., LALBAKSHI, A. Improved microstrip hairpin-line bandpass filters for spurious response suppression. *Electronic Letters*, 2012, vol. 48, no. 14, p. 858–859. DOI: 10.1049/el.2012.0967
- [9] HUANG, T., SHAO, Z. A size-miniaturized bandpass filter with selectivity-enhanced and high harmonic suppression performance. *International Journal of Microwave and Wireless Technologies*, 2017, vol. 9, p. 1809–1815. DOI: 10.1017/S1759078717000587
- [10] HUANG, T., SHAO, Z. H., CHEN, Z. Miniaturized wideband bandpass filter with enhanced selectivity and stopband suppression. *Microwave and Optical Technology Letters*, 2018, vol. 60, p. 769–772. DOI: 10.1002/mop.31052
- [11] CHATTERJEE, S., DAS, T. K. Compact hairpin-line bandpass filter with harmonic suppression by periodic grooves. In *Proceedings of Mediterranean Microwave Symposium (MMS)*. Hammamet (Tunisia), 2019, p. 1–4. DOI: 10.1109/MMS48040.2019.9157328
- [12] NGUYEN, C., HSIEH, C., BALL, D. W. Millimeter wave printed circuit spurline filters. In *IEEE MTT-S International Microwave Symposium Digest*. Boston (MA, USA), 1983, p. 98–100. DOI: 10.1109/MWSYM.1983.1130821
- [13] LIU, H., SUN, L., SHI, Z. Dual-bandgap characteristics of spur-line filters and its circuit modeling. *Microwave and Optical Technology Letters*, 2007, vol. 49, no. 11, p. 2805–2807. DOI: 10.1002/mop.22862

About the Authors ...

Tarun Kumar DAS was born in Kolkata, India, in 1979. Currently he is working toward the Ph.D. degree at Jadavpur University. His research areas include harmonic suppression in compact microwave filters.

Sayan CHATTERJEE was born in Kolkata, India, in 1980. Currently, he is working as an Associate Professor in Jadavpur University, India. His research interests include microwave filters and antennas.